Available online at www.sciencedirect.com
ScienceDirect
Journal of the European Ceramic Society 29 (2009) 1109–1117
www.elsevier.com/locate/jeurceramsoc

Ag^+- and Zn^{2+}-exchange kinetics and antimicrobial properties of 11 Å tobermorites

Nichola J. Coleman *, Alistair H. Bishop, Samantha E. Booth, John W. Nicholson

School of Science, University of Greenwich, Chatham Maritime, Kent ME4 4TB, United Kingdom

Received 6 April 2008; received in revised form 11 August 2008; accepted 12 August 2008
Available online 24 September 2008

Abstract

Ag^+- and Zn^{2+}-exchanged zeolites and clays have been used as coatings and in composites to confer broad-spectrum antimicrobial properties on a range of technical and biomedical materials. 11 Å tobermorite is a bioactive layer lattice ion exchanger whose potential as a carrier for Ag^+ and Zn^{2+} ions in antimicrobial formulations has not yet been explored. In view of this, batch Ag^+- and Zn^{2+}-exchange kinetics of two structurally distinct synthetic 11 Å tobermorites and their subsequent bactericidal action against *Staphylococcus aureus* and *Pseudomonas aeruginosa* are reported. During the exchange reactions, Ag^+ ions were found to replace labile interlayer cations; whereas, Zn^{2+} ions also displaced structural Ca^{2+} ions from the tobermorite lattice. In spite of these different mechanisms, a simple pseudo-second-order model provided a suitable description of both exchange processes ($R^2 \geq 0.996$). The Ag^+- and Zn^{2+}-exchanged tobermorite phases exhibited marked bacteriostatic effects against both bacteria, and accordingly, their potential for use as antimicrobial materials for *in situ* bone tissue regeneration is discussed.

Keywords: Chemical properties; Biomedical applications; Silicate; Pseudo-second-order kinetics

1. Introduction

Tobermorites are a family of naturally occurring layered calcium silicate hydrate cation exchangers which are also readily synthesised from a variety of reagents under hydrothermal conditions.[1–6] Their ideal structures comprise infinite double layers of seven-coordinated Ca–O polyhedra linked on both sides to wollastonite-like silicate chains running along the *b*-axis direction, as depicted in Fig. 1.[7,8] This assembly is stacked in the *c*-direction creating interlayer channels, similar to those found in zeolites, which accommodate water molecules and one labile calcium ion *per* unit formula. Paired silicate tetrahedra facing into the polyhedral calcium layer are referred to as 'non-bridging', whereas those tetrahedra which link the pairs together are termed 'bridging'. Deviations from ideal structure, such as breaks in the silicate chains and the condensation of bridging silicate tetrahedra between adjacent layers, arise from stacking defects and crystallographic substitutions give rise to compositional variations which influence cation exchange behaviour.[2–4]

Members of the tobermorite family are characterised in terms of their interlayer spacing which is dependent on the number of water molecules *per* unit formula. There are three principal polytypes, *viz.* 9, 11 and 14 Å, whose names are derived according to the approximate *d*-spacing of their (0 0 2) Bragg reflections (i.e. their basal spacings). 11 Å tobermorite, $Ca_5Si_6O_{16}(OH)_2 \cdot 4H_2O$, the most technologically-significant polytype, is found among alteration products formed at the cement rock interface of toxic and nuclear waste repositories and is the principal binder in autoclaved concrete products. During the past 20 years, aspects of the ion exchange characteristics of a range of natural and synthetic 11 Å tobermorites have been investigated with respect to their application in nuclear and hazardous wastewater treatment.[2–4] 11 Å tobermorite has also been investigated as a heterogeneous catalyst for lactose isomerisation,[5] and the incorporation of tobermorite nanofibres into bioactive composites for bone tissue regeneration has been suggested.[9]

The broad-spectrum antimicrobial properties of the silver (I) ion, Ag^+, have been utilised since ancient times by the Mediterranean and Asiatic cultures and the historic use of silver foils in the surgical treatment of wounds and broken bones is documented.[10] Silver-exchanged zeolites and clays have been

* Corresponding author.
E-mail address: nj_coleman@yahoo.co.uk (N.J. Coleman).

0955-2219/$ – see front matter © 2008 Elsevier Ltd. All rights reserved.
doi:10.1016/j.jeurceramsoc.2008.08.015

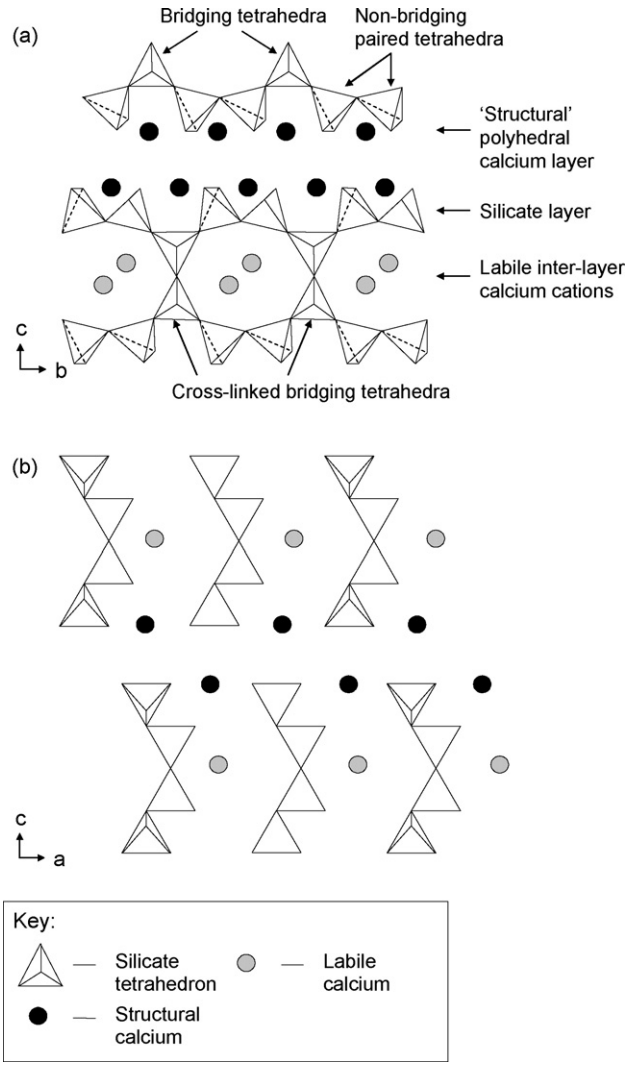

Fig. 1. Projections of 11 Å tobermorite (a) in the *bc*-plane and (b) in the *ac*-plane.

used as coatings and in composites to confer antimicrobial properties to dental filling materials,[11] Portland cement mortars,[12] food packaging,[13,14] ointments,[15] stainless steel,[16] paper, paints and plastic products.[17] The antibacterial properties of silver have also been exploited by its incorporation into ceramic and glass implant materials for prosthesis and tissue regeneration.[18–20] Furthermore, silver nanoparticles, complexes, chelates and their composites have been shown to afford antibacterial action against a wide range of pathogens in various technical and biomedical applications.[10,21–23]

Zinc is an essential antioxidant and anti-inflammatory agent in the human body, deficiency in which causes delayed wound healing, immune dysfunction, growth retardation and neurosensory disorders. In the human body Zn^{2+} ions are associated with the structure and function of a large number of macromolecules and are essential to over 300 enzymic processes which include the regulation of bone growth and the replication of DNA.[24,25] The antimicrobial action of the Zn^{2+} ion is less extensive than that of Ag^{+} although its wound healing and bactericidal properties are similarly exploited in a range of formulations, composites and coatings.[16,17,26]

The ion exchange and antimicrobial characteristics of numerous Ag^{+}- and Zn^{2+}-bearing zeolites and clays have been researched although, to date, there have been no such reports of the antibacterial properties of Ag^{+}- and Zn^{2+}-bearing tobermorites. Tobermorites have a number of technical advantages over zeolites and clays in that they can be prepared, not only as finely dispersed powders, but also as nanofibres and large monolithic articles of variable porosity. Tobermorites are stable in Portland cement mortars, whereas zeolites and clays degrade by pozzolanic reaction. And furthermore, the recent discovery that tobermorite fibres exhibit bioactivity – the ability to bond to living bone tissue – has invoked interest in their incorporation into composites for bone tissue engineering.[9]

In the present study, batch Ag^{+}- and Zn^{2+}-exchange kinetics of two structurally distinct 11 Å tobermorite samples are modelled using simple pseudo-first- and pseudo-second-order rate equations. A preliminary *in vitro* investigation of the antibacterial action of the Ag^{+}- and Zn^{2+}-bearing tobermorites against *Staphylococcus aureus* and *Pseudomonas aeruginosa* is also reported. *S. aureus* and *P. aeruginosa* were selected for this investigation as they are known to cause biomaterial centred infections and resistant septic conditions in tissues such as bones, teeth and skin.[19]

2. Experimental

2.1. Hydrothermal synthesis of 11 Å tobermorite specimens

11 Å tobermorite specimens were prepared in duplicate by heating mixtures of 6.8 g of $Na_2SiO_3 \cdot 5H_2O$, 1.47 g of CaO and 60 cm^3 of NaOH solution at 100 °C in sessile hermetically sealed PTFE reaction vessels under autogenous pressure for 19 days. Samples Tob-Na1 and Tob-Na4 were synthesised in 1.0 M and 4.0 M $NaOH_{(aq)}$, respectively. The products of each synthesis were washed with deionised water to pH 7, dried to constant mass in air at 40 °C and stored in air-tight polypropylene containers until required. Analysis of the reaction products by powder XRD and ^{29}Si MAS NMR is described elsewhere.[27] Oxide analyses were obtained by X-ray fluorescence spectroscopy (XRF) which was carried out at the Materials Research Institute, Sheffield Hallam University, Sheffield, S1 1WB, UK.

2.2. Evaluation of the silicate chain structure by ^{29}Si MAS NMR

Notation will be used to describe the silicate chain structure such that the symbol Q represents one SiO_4^{4-} tetrahedron and a superscript denotes the number of other Q units to which it is bonded. For example, a mid-chain SiO_4^{4-} unit would be represented as Q^2.

The silicate chain configurations of specimens Tob-Na1 and Tob-Na4 were evaluated in terms of their 'mean chain length' (MCL). MCL is a measure of the average number of tetrahedra linked along the *b*-axis direction between breaks in the chain (including bridging, cross-liked and non-bridging tetrahedra)

and is given by

$$\mathrm{MCL} = \frac{2(Q^1 + Q^2 + Q^3)}{Q^1}$$

where the Q^n symbols represent the relative intensities of the ^{29}Si resonances arising from the corresponding silicate tetrahedra.

2.3. Ag^+ and Zn^{2+} ion exchange kinetics

The ion exchange kinetics for the uptake of Ag^+ and Zn^{2+} by Tob-Na1 and Tob-Na4 were determined in triplicate in sessile batch sorption experiments using single metal nitrate solutions at 25 °C. In each case, 0.5 g of tobermorite were added to 0.2 dm^{-3} of either 3.0 mM $AgNO_{3(aq)}$ or 5.0 mM $Zn(NO_3)_{2(aq)}$ in a screw-capped polypropylene bottle. Residence times for specimens varied between 15 min and 9 days, after which the supernatant liquors and ion exchanged solids were separated by gravitational filtration. The recovered solutions were appropriately diluted and analysed for silver and zinc by atomic absorption spectroscopy using a Pye Unicam SP 9 spectrophotometer. The resulting Ag^+- and Zn^{2+}-substituted tobermorites (Tob-Ag1 and Tob-Zn1 derived from Tob-Na1; and Tob-Ag4 and Tob-Zn4 derived from Tob-Na4) were dried to constant mass in air at 40 °C and analysed by XRF.

2.4. Kinetic models

The pseudo-first-order rate model which describes the sorption of a solute by a solid surface can be expressed in the following way[28–30]:

$$\frac{dq_t}{dt} = k_1(q_e - q_t)$$

where k_1 is the apparent pseudo-first-order rate constant (in min^{-1}), q_t is the extent of sorption at time t (in mmol g^{-1}), and q_e is the extent of sorption at equilibrium (in mmol g^{-1}). This pseudo-rate law is used to describe processes in which the reaction rate, dq_t/dt, is proportional to the number of available sorption sites ($q_e - q_t$). The linear, integrated form of this equation for the boundary conditions; $q_t = 0$ at $t = 0$ and $q_t = q_t$ at $t = t$, can be written as

$$\log(q_e - q_t) = \log q_e - \frac{k_1}{2.303}t.$$

Hence, the pseudo-first-order rate equation is obeyed when a linear relationship exists between $\log(q_e - q_t)$ and t, in which case, k_1 may be estimated from the gradient of the plot.

Similarly, the pseudo-second-order rate expression can be used to describe sorption processes in which the reaction rate is proportional to the square of the number of available sorption sites[28–31]:

$$\frac{dq_t}{dt} = k_2(q_e - q_t)^2$$

where k_2 is the apparent pseudo-second-order rate constant (in g $mmol^{-1}$ min^{-1}), and can be rearranged thus:

$$\frac{t}{q_t} = \frac{1}{k_2 q_e^2} + \frac{1}{q_e}t.$$

Estimates of k_2 and q_e may be derived from the intercept and gradient of a linear plot of t/q_t against t.

The simple kinetic models outlined above have been widely applied to the uptake of a range of solutes by a variety of sorbent and ion exchange substrates.[28–31] They have been used to compare ion exchange efficiencies and to predict the performance of sorption processes although the relationship between the models and the underlying sorption mechanisms is disputed. However, Azizian[32] presents a compelling theoretical argument which suggests that the applicability of the kinetic model does not arise from a fundamental difference in sorption mechanism, but is in fact a function of initial solute concentration. His proof indicates that high solute concentrations (with respect to the number of active sorption sites) give rise to apparent pseudo-first-order kinetics and that pseudo-second-order kinetics become more relevant as initial solute concentration decreases. In each case, the apparent rate constant is a combination of the adsorption and desorption rate constants, although k_1 is shown to be a linear function of initial solute concentration whereas k_2 is a more complex function of this parameter.

2.5. Antibacterial assays

Samples Tob-Na1, Tob-Na4, Tob-Ag1, Tob-Ag4, Tob-Zn1 and Tob-Zn4 at concentrations of 1.0 mg cm^{-3} and 10.0 mg cm^{-3} were added in triplicate to separate McCartney bottles containing 10 cm^3 of Nutrient Broth (Oxoid). These tubes were then inoculated with cultures of *S. aureus* NCIMB 9518 or *P. aeruginosa* NCIMB 8628 to densities of 4.1×10^4 and 5.6×10^6 colony forming units per cm^3, respectively. The cultures were then incubated, with shaking, at 37 °C overnight and duplicate plate counts on nutrient both (Oxoid) were taken for each assay. Cultures with no added tobermorite were also analysed as controls.

Viable cell count data for the cultures containing tobermorite samples were compared with those of the control culture populations. In each case, the null hypothesis that the two measurements are not significantly different was tested at the 95% significance level using a one-tailed t-test. The observed value of t was estimated as

$$t = \frac{\bar{x}_d\sqrt{n}}{s_d}$$

where n is the number of data pairs, $\bar{x}_d$ is the mean of the differences between the data pairs and s_d is the standard deviation of $\bar{x}_d$. If the tabulated critical t-value was found to be greater than the observed (calculated) value of $|t|$, the null hypothesis was retained (i.e. the two sets of results were not statistically different).

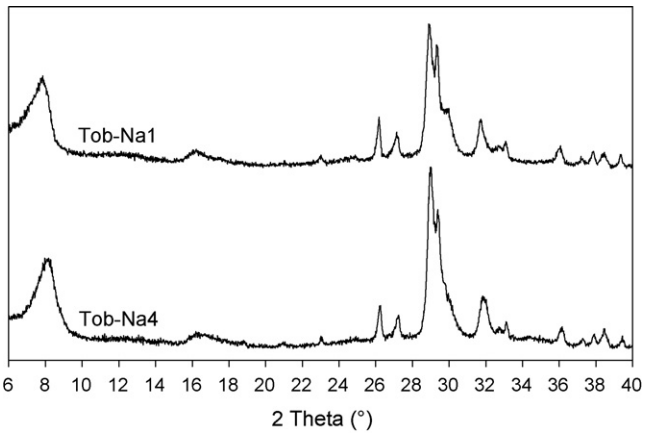

Fig. 2. Powder XRD patterns of Tob-Na1 and Tob-Na4.

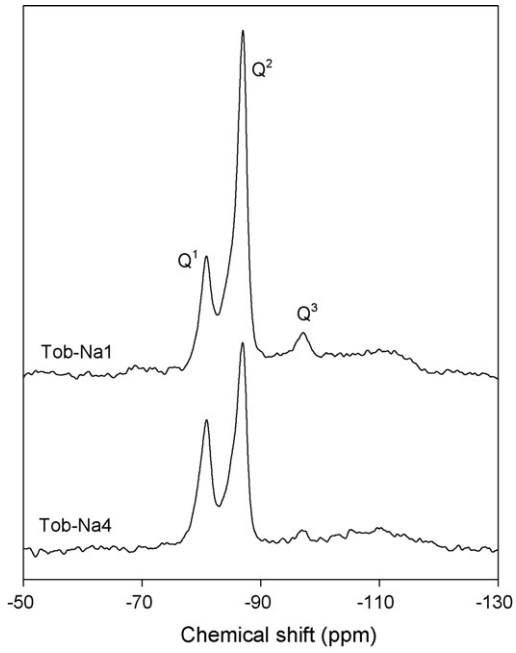

Fig. 3. ^{29}Si MAS NMR spectra of Tob-Na1 and Tob-Na4.

3. Results and discussion

3.1. Characterisation of Tob-Na1 and Tob-Na4

The powder XRD data for specimens Tob-Na1 and Tob-Na4 (Fig. 2) are similar to those of other synthetic phase-pure crystalline 11 Å tobermorites reported in the literature.[1,9,33] Minor traces of calcite ($CaCO_3$) are also present and commonly arise from atmospheric carbonation during the preparation of tobermorites. The ^{29}Si MAS NMR data for specimens Tob-Na1 and Tob-Na4 (Fig. 3) are also consistent with those of crystalline phase-pure 11 Å tobermorites.[34,35] Mid-chain Q^2 silicate tetrahedra of the wollastonite-like chains are denoted by the asymmetrical resonances at −86.5 ppm and the signals at −97.0 arise from bridging Q^3 silicate tetrahedra which are linked across the interlayer (Fig. 3). Q^1 resonances are signified by the peaks at −80.5 ppm which arise from breaks along the silicate chains and the presence of isolated dimers,[35] and the broad low-intensity signals at ∼−110 ppm are assigned to traces of Q^4 amorphous silica.

The mean silicate chain lengths of specimens Tob-Na1 and Tob-Na4 are estimated to be 9.7 and 5.5 silicate units, respectively. Hence, the Tob-Na4 specimen prepared in 4 M $NaOH_{(aq)}$ is less well crystallised than Tob-Na1 which was prepared in 1 M $NaOH_{(aq)}$. Other research has demonstrated that the first reaction product during tobermorite synthesis is a poorly organised calcium silicate hydrate gel phase and that increasing concentrations of Na^+ ions in the reaction mixture can stabilise this intermediate phase and inhibit the subsequent development of a well-crystallised tobermorite product.[4,33] Therefore, the comparatively fragmented chain system of specimen Tob-Na4 is consistent with the mixture composition-structure relationships reported previously.

The calculated formulae for specimens Tob-Na1 and Tob-Na4, derived from XRF analysis, are listed in Table 1. It is of interest to note that, despite the increased Na^+ ion concentration in the reaction mixture, the extent of Na^+ substitution in the latter specimen is ∼23% lower than that of its counterpart.

3.2. Ag^+ and Zn^{2+} ion exchange kinetics

The uptake profiles for Ag^+ by the tobermorite specimens are plotted in Fig. 4 and show that equilibrium is achieved within 24 h, by which time the extents of Ag^+-uptake by Tob-Na1 and Tob-Na4 are found to be 10.4 and 10.7 wt% (0.958 and 0.993 mmol g^{-1}), respectively. These equilibrium silver-contents exceed those reported for palygorskite (0.6 wt%)[36] and montmorillonite (8.37 wt%)[37] clays and fall within the range reported for various clinoptilolites (3–18.4 wt%).[38–40]

Table 1
Formulae of the tobermorite specimens, percentages of Ca^{2+} and Na^+ ions which were exchanged for Ag^+ or Zn^{2+} ions and the Ag^+- and Zn^{2+}-content of the exchanged tobermorites

Sample	Formula	Ca exchanged (%)	Na exchanged (%)	Ag- or Zn-content (wt%)
Tob-Na1	$Ca_{4.55}Na_{0.44}Si_{6.00}O_{16.77}$ 6.4H_2O	–	–	–
Tob-Na4	$Ca_{4.38}Na_{0.34}Si_{6.00}O_{16.55}$ 5.9H_2O	–	–	–
Tob-Ag1	$Ca_{4.06}Na_{0.04}Ag_{0.92}Si_{6.00}O_{16.54}$ 11.9H_2O	11	91	10.4
Tob-Ag4	$Ca_{4.07}Na_{0.04}Ag_{0.93}Si_{6.00}O_{16.56}$ 10.6H_2O	7	88	10.7
Tob-Zn1	$Ca_{3.19}Na_{0.07}Zn_{1.99}Si_{6.00}O_{17.21}$ 5.4H_2O	30	84	12.4
Tob-Zn4	$Ca_{3.23}Na_{0.05}Zn_{1.59}Si_{6.00}O_{16.85}$ 3.1H_2O	26	85	10.7

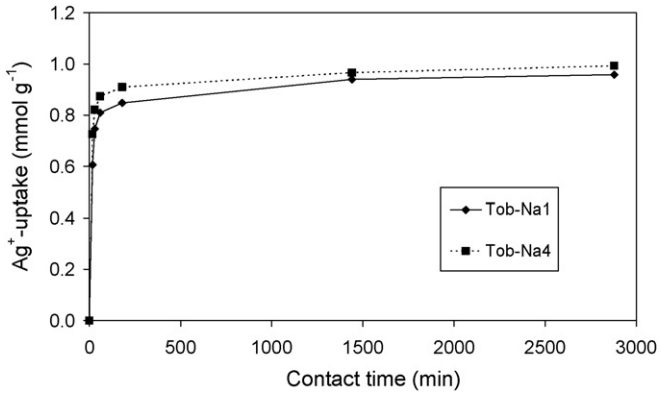

Fig. 4. Uptake of Ag^+ ions by Tob-Na1 and Tob-Na4.

XRF analysis of the Ag^+-exchanged tobermorite phases, *viz.* Tob-Ag1 and Tob-Ag4, indicated that 91% and 88% of the original Na^+ ions had been exchanged for incoming Ag^+ ions, as had 11% and 7% of the original Ca^{2+} ions, respectively (Table 1). These data suggest that the majority of labile interlayer Na^+ and Ca^{2+} ions in both tobermorite samples is readily exchanged for Ag^+ ions, and that the remaining four Ca^{2+} ions *per* unit formula which constitute the structural Ca–O polyhedral layer are not available for reaction with Ag^+ under the selected experimental conditions (Table 1).

The applicability of the pseudo-first- and pseudo-second-order kinetic models (outlined in Section 2.4) to the uptake of Ag^+ by Tob-Na1 and Tob-Na4 has been tested by fitting the experimental data to the models by least squares regression analysis. The apparent pseudo-rate constants, integrated rate equations, experimental and calculated equilibrium uptake values and the corresponding squares of the correlation coefficients (R^2) are listed in Table 2. A strong correlation between the experimental data and the pseudo-second-order kinetic model is indicated by $R^2 = 0.9999$ in each case; whereas the pseudo-first-order model is, in comparison, shown to be less representative ($0.745 \leq R^2 \leq 0.575$). Furthermore, the theoretical steady-state uptake values, $q_{e,calc}$, obtained by the pseudo-second-order model, 0.961 mmol g^{-1} and 0.993 mmol g^{-1} for Tob-Na1 and Tob-Na4, respectively, are within 1% of the experimentally observed data, $q_{e,exp}$ (Table 2). The experimental data for Ag^+-uptake and theoretically fitted lines for the pseudo-first- and pseudo-second-order kinetic models are presented in Fig. 5(a) and (b), respectively.

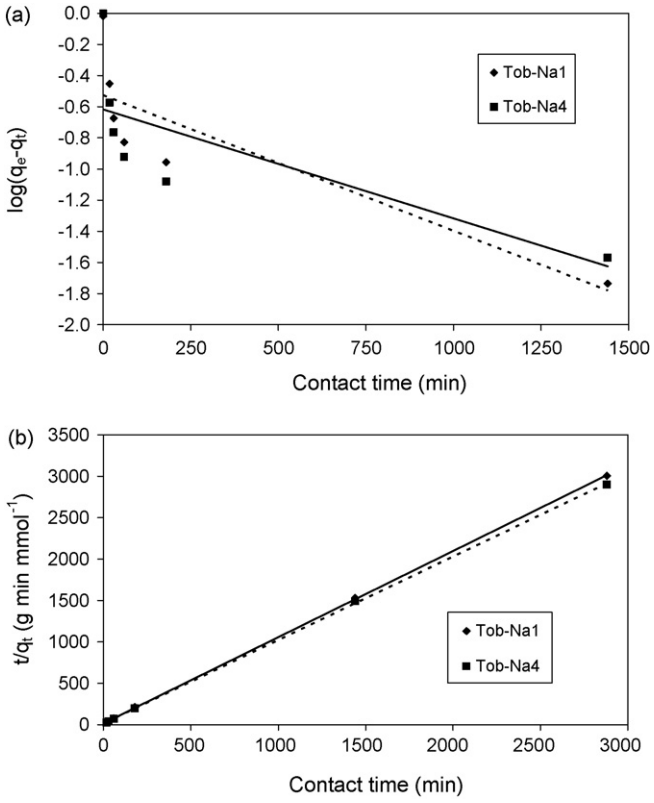

Fig. 5. Kinetic models fitted to experimental data for the uptake of Ag^+ by Tob-Na1 and Tob-Na4: (a) pseudo-first-order model and (b) pseudo-second-order model.

To date, no citations for the application of these pseudo-kinetic models to describe the uptake of Ag^+ by clays, zeolites or other layered silicate materials could be located in the literature. However, other researchers have reported that the uptake of Ag^+ ions by modified chitosan, a biopolymeric sorbent whose potential applications include antimicrobial dressings for burns and wounds, also conforms to the pseudo-second-order kinetic model.[41–43] The respective pseudo-second-order rate constants, k_2, for the uptake of Ag^+ ions by Tob-Na1 and Tob-Na4, 0.067 and 0.079 g $mmol^{-1}$ min^{-1}, determined in the present study, show that these exchange reactions are approx-

Table 2
Kinetic data for the uptake of Ag^+ ions by Tob-Na1 and Tob-Na4

Sample	k_1 ($\times 10^3$ min^{-1})	Integrated rate equation	$q_{e,exp}$ (mmol g^{-1})	$q_{e,calc}$ (mmol g^{-1})	R^2
Pseudo-first-order model					
Tob-Na1	2.01	$\log(q_e - q_t) = -(8.72 \times 10^{-4})t - 0.527$	0.958 (±0.033)[a]	0.298	0.745
Tob-Na4	1.61	$\log(q_e - q_t) = -(7.00 \times 10^{-4})t - 0.618$	0.993 (±0.029)[a]	0.241	0.575
Sample	k_2 (g $mmol^{-1}$ min^{-1})				
Pseudo-second-order model					
Tob-Na1	0.0671	$t/q_t = 1.04t + 16.2$	0.958 (±0.033)[a]	0.961	0.9999
Tob-Na4	0.0792	$t/q_t = 1.01t + 12.8$	0.993 (±0.029)[a]	0.993	0.9999

[a] Figures in brackets are the 95% confidence limits of the mean equilibrium Ag^+-uptake values, $q_{e,exp}$.

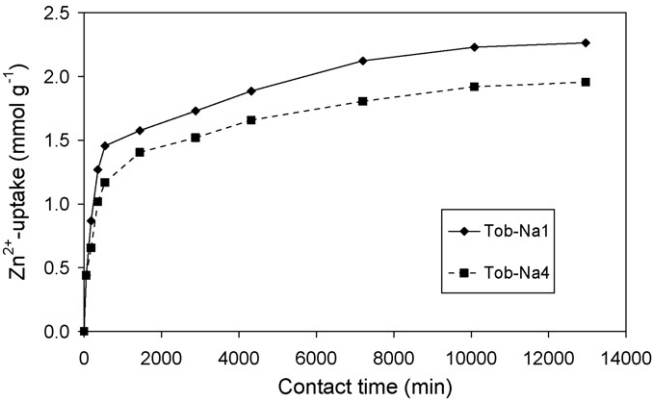

Fig. 6. Uptake of Zn^{2+} ions by Tob-Na1 and Tob-Na4.

imately twice as fast as that reported for modified chitosan ($k_2 = 0.033\ g\ mmol^{-1}\ min^{-1}$).[39]

A previous study of the rate of uptake of Cd^{2+} by 11 Å tobermorites has indicated that structural disorder within the lattice accelerates ion exchange kinetics but has little impact on the total number of available exchange sites.[4] This observation is also reflected in the present findings, since k_2 for the uptake of Ag^+ by the more poorly organised Tob-Na4 lattice is approximately 15% greater than that of its more crystalline counterpart (Table 2).

The uptake profiles for Zn^{2+} ions by Tob-Na1 and Tob-Na4 are depicted in Fig. 6 and indicate that equilibrium is not established within the 216-h observation period, by which time Zn^{2+}-uptake is found to be 12.4 wt% and 10.7 wt% (2.26 mmol g^{-1} and 1.95 mmol g^{-1}), respectively. XRF analysis demonstrated that, in addition to the exchange of labile cations as is observed in the case of Ag^+-uptake, approximately 20% of the 'structural' Ca^{2+} ions from the polyhedral layer also participate in the Zn^{2+} exchange process (Table 1). This difference in mechanism between Ag^+- and Zn^{2+}-exchange accounts for the superior uptake capacity of tobermorites for Zn^{2+} and for their comparatively slow reaction rates, since bond-breaking processes and structural rearrangement of the lattice occur during Zn^{2+}-uptake. Unlike those of Ag^+ and Cd^{2+},[4] the rate and extent of Zn^{2+}-uptake are significantly greater for the more crystalline Tob-Na1 specimen ($P = 0.01$); an observation that is also likely to derive from the participation of structural Ca^{2+} ions from the Ca–O double layer during the Zn^{2+} exchange reactions.

Integrated forms of the pseudo-first- and pseudo-second-order rate equations for the uptake of Zn^{2+} by Tob-Na1 and Tob-Na4, apparent pseudo-rate constants, k_1 and k_2, and the corresponding squares of the correlation coefficients, R^2, are listed in Table 3 along with experimental and theoretical Zn^{2+}-uptake values following a contact time of 216 h, $q_{t\ at\ 216\ h,exp}$ and $q_{t\ at\ 216\ h,calc}$, respectively. High correlations between the experimental data and the pseudo-second-order kinetic model for the uptake of Zn^{2+} by Tob-Na1 and Tob-Na4 are indicated by respective R^2 values of 0.996 and 0.997. Furthermore, calculated uptake values, $q_{t\ at\ 216\ h,calc}$, obtained by the pseudo-second-order model are within 2% of the experimentally observed data. R^2 values of 0.955 were obtained by fitting the Zn^{2+}-uptake data to the pseudo-first-order model, and indicate that this model is less representative (Table 3). The relationships between the experimental Zn^{2+}-uptake data and the theoretically fitted curves for these kinetic models are shown in Fig. 7.

Typical equilibrium times for Zn^{2+}-uptake by clays (stevensite[44] and bentonite[45]) and zeolites (A,[46] 4A,[45] 13X[45]) are within 2 h of contact and maximum sorption capacities are generally found to be between 0.3 mmol g^{-1} and 2.5 mmol g^{-1}. A number of studies has shown that the pseudo-second-order model is representative of these processes and k_2 values in the range 8.3×10^{-3} to 15.43 g $mmol^{-1}\ min^{-1}$ are reported.[44–46] In comparison, the Zn^{2+}-exchange rates for Tob-Na1 ($k_2 = 8.50 \times 10^{-4}\ g\ mmol^{-1}\ min^{-1}$) and Tob-Na4 ($k_2 = 9.87 \times 10^{-4}\ g\ mmol^{-1}\ min^{-1}$) are considerably slower than those documented in the literature; however, the extents of Zn^{2+}-uptake by the tobermorite specimens were found to be towards the top end of the reported range for clays and zeolites.[44–46]

3.3. Antibacterial properties of Ag^+- and Zn^{2+}-exchanged tobermorites

The results of the preliminary *in vitro* antibacterial assays, listed in Table 4, indicate that the original tobermorite specimens, Tob-Na1 and Tob-Na4, exhibit modest inhibitory effects against both *P. aeruginosa* and *S. aureus* at the selected concentrations of 1.0 and 10.0 mg cm^{-3}, although in general the viable cell counts in the presence of these unsubstituted tobermorites were only found to be one or two orders of magnitude lower than those of the control populations. In contrast, marked inhibitory effects were noted for all Ag^+- and Zn^{2+}-bearing

Table 3
Kinetic data for the uptake of Zn^{2+} ions by Tob-Na1 and Tob-Na4

Sample	k_1 ($\times 10^4\ min^{-1}$)	Integrated rate equation	$q_{t\ at\ 216\ h,exp}$ (mmol g^{-1})	$q_{t\ at\ 216\ h,calc}$ (mmol g^{-1})	R^2
Pseudo-first-order model					
Tob-Na1	1.55	$\log(q_e - q_t) = -(1.48 \times 10^{-4})_t + 0.103$	2.26 (±0.04)[a]	1.46	0.955
Tob-Na4	3.42	$\log(q_e - q_t) = -(1.55 \times 10^{-4})_t + 0.169$	1.95 (±0.06)[a]	1.25	0.955
Sample	k_2 ($\times 10^4$ g $mmol^{-1}\ min^{-1}$)				
Pseudo-second-order model					
Tob-Na1	8.50	$t/q_t = 0.433t + 220$	2.26 (±0.04)[a]	2.22	0.996
Tob-Na4	9.87	$t/q_t = 0.502t + 255$	1.95 (±0.06)[a]	1.92	0.997

[a] Figures in brackets are the 95% confidence limits of the mean Zn^{2+}-uptake values after a contact time of 216 h, $q_{t\ at\ 216\ h,exp}$.

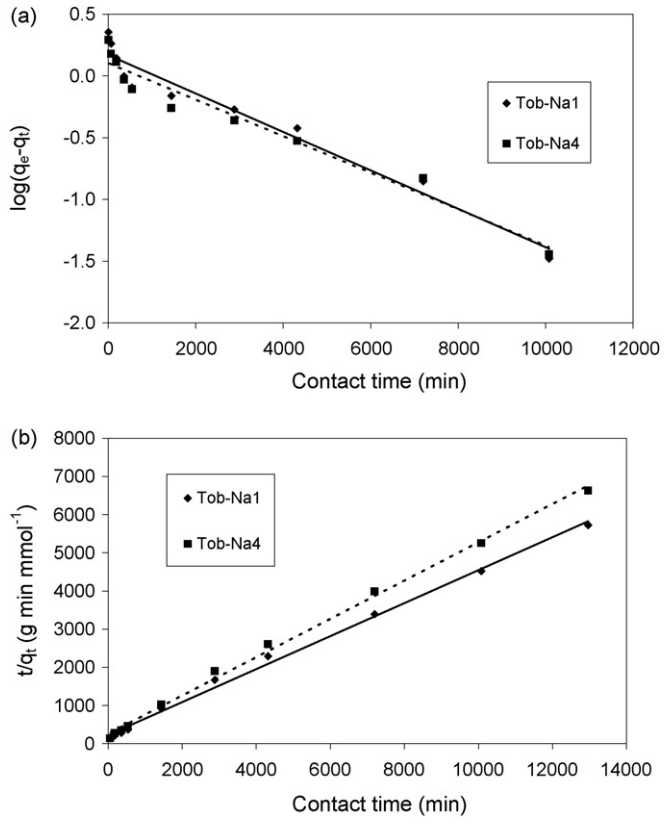

Fig. 7. Kinetic models fitted to experimental data for the uptake of Zn^{2+} by Tob-Na1 and Tob-Na4: (a) pseudo-first-order model and (b) pseudo-second-order model.

tobermorites against *S. aureus* at both concentrations. In each case, the Ag^{+}- and Zn^{2+}-substituted tobermorites were found to reduce the *S. aureus* cell populations by more than five orders of magnitude relative to those of the control culture. Similarly, all Ag^{+}- and Zn^{2+}-substituted tobermorites at concentrations of 10.0 mg cm^{-3} were also found to effect a relative reduction in the *P. aeruginosa* population by greater than five orders of magnitude. However, the inhibitory effect of these Ag^{+}- and Zn^{2+}-exchanged tobermorites against *P. aeruginosa* at 1.0 mg cm^{-3} was less pronounced and, in fact, the extent of bacterial growth in the presence of Tob-Zn4 was found to be greater than that of the control population.

In summary, the results of these antibacterial assays demonstrate that each of the Ag^{+}- and Zn^{2+}-bearing tobermorite samples exhibits marked bacteriostatic effects against both *S. aureus* and *P. aeruginosa*, although their antimicrobial efficiencies differ between the two bacteria. These initial findings indicate that, in the case of *S. aureus*, the minimum inhibiting concentrations (MICs) of these substituted tobermorites are below 1.0 mg cm^{-3} and that their MICs with respect to *P. aeruginosa* are in the range 1.0–10.0 mg cm^{-3}.

3.4. Potential applications of Ag^{+}- and Zn^{2+}-exchanged tobermorites

In general, the body's defence mechanism will stimulate the formation of a fibrous capsule around an artificial implant material in an attempt to isolate it from the surrounding tissue; however, certain bioactive glasses and ceramics have been shown to form stable mechanically compliant bonds with living bone tissue *in vivo*.[47] The bioactive material-cell interface usually develops *via* the deposition of a layer of substituted hydroxycarbonate apatite (HCA), $(Ca,Na)_{10}(PO_4,CO_3)_6(OH)_2$, which forms by the precipitation of ions present in human plasma. The resulting superficial HCA layer is similar in structure to the mineral component of bone and provides a focus for the attachment and proliferation of new bone-forming cells. These bioactive materials can be used to repair diseased or damaged bone tissue and can be designed to remain *in situ* indefinitely or to degrade as the nor-

Table 4
Cell count data for control cultures and cultures containing Tob-Na1, Tob-Na4, Tob-Ag1, Tob-Ag4, Tob-Zn1 and Tob-Zn4

Culture	Control	Tob-Na1	Tob-Na4	Tob-Ag1	Tob-Ag4	Tob-Zn1	Tob-Zn4
Staphylococcus aureus NCIMB 9518							
1.0 mg Tob cm^{-3}							
Mean (CFU cm^{-3})	4.7×10^9	2.7×10^8	4.6×10^8	No count (10^4)	No count (10^4)	No count (10^4)	No count (10^4)
St. dev. (CFU cm^{-3})	3.0×10^9	2.7×10^8	2.2×10^8	–	–	–	–
Observed $\|t\|$[a]	–	3.66	3.41	–	–	–	–
10.0 mg Tob cm^{-3}							
Mean (CFU cm^{-3})	4.7×10^9	3.6×10^9	2.0×10^7	No count (10^4)	No count (10^4)	No count (10^4)	No count (10^4)
St. dev. (CFU cm^{-3})	3.0×10^9	2.0×10^9	2.0×10^7	–	–	–	–
Observed $\|t\|$[a]	–	1.02	3.87	–	–	–	–
Pseudomonas aeruginosa NCIMB 8628							
1.0 mg Tob cm^{-3}							
Mean (CFU cm^{-3})	9.3×10^{10}	1.25×10^9	5.3×10^9	7.1×10^9	8.2×10^9	6.3×10^9	9.7×10^9
St. dev. (CFU cm^{-3})	2.2×10^{10}	0.93×10^9	2.5×10^9	1.8×10^9	3.9×10^9	2.2×10^9	1.5×10^9
Observed $\|t\|$[a]	–	7.78	4.37	2.65	6.37	4.98	3.90
10.0 mg Tob cm^{-3}							
Mean (CFU cm^{-3})	9.3×10^{10}	4.8×10^9	1.00×10^{10}	No count (10^4)	No count (10^4)	No count (10^4)	No count (10^4)
St. dev. (CFU cm^{-3})	2.2×10^{10}	1.9×10^9	0.22×10^{10}	–	–	–	–
Observed $\|t\|$[a]	–	4.55	5.11	–	–	–	–

[a] Critical $|t|$ at ($P = 0.10$) for ($n - 1$) degrees of freedom is 2.02.

mal functions of the host tissue are restored. Lin and co-workers have recently acknowledged that tobermorite fibres exhibit the property of bioactivity and their research indicates that the tobermorite lattice will stimulate bone tissue regeneration and subsequently degrade in the physiological environment.[9]

The occurrence of biomaterial-centred sepsis restricts the scope and success of bioactive implants and accordingly the problems presented by infection following implant surgery have stimulated research into the development of bioactive materials with antimicrobial properties.[18–20] Hence, on the basis of this preliminary study, it is envisaged that Ag^+- and Zn^{2+}-exchanged tobermorites may exhibit the combined bioactive and bacteriostatic characteristics which are required for successful tissue integration. Additionally, it is anticipated that the wound healing properties of the Zn^{2+} ion may also be relevant in a biomaterials context. Further work to confirm whether the bioactivity and biocompatibility of tobermorites is compromised by the presence of the interlayer Ag^+ and Zn^{2+} ions is currently underway.

As previously mentioned, Ag^+- and Zn^{2+}-exchanged clays and zeolites have been incorporated into a range of materials which exploit their antimicrobial properties,[11–23] and in addition, these Ag^+-substituted materials also find application in electro- and photocatalysis.[48,49] Hence, it is anticipated that Ag^+-substituted 11 Å tobermorites may also be potential candidates for incorporation into electro- and photocatalytic cells and nanocapacitors.

4. Conclusions

Labile interlayer Na^+ and Ca^{2+} ions in 11 Å tobermorites are readily exchanged for Ag^+ ions from solution under batch conditions at 25 °C; whereas, Zn^{2+} ions are exchanged for both labile cations and 'structural' Ca^{2+} ions from the polyhedral Ca–O layer within the tobermorite lattice. Despite these different mechanisms, a simple pseudo-second-order model can be used to describe both exchange processes ($R^2 \geq 0.996$). The resulting Ag^+- and Zn^{2+}-exchanged phases exhibit marked bacteriostatic action against *S. aureus* and *P. aeruginosa*, and are potentially significant to a range of applications, including antimicrobial materials for bone tissue regeneration.

Acknowledgements

It is with gratitude that NJC acknowledges financial support for this research from the Royal Society of Chemistry and from The Royal Society.

References

1. Kalousek, G. L., Crystal chemistry of hydrous calcium silicates. 1. Substitution of aluminium in lattice of tobermorite. *J. Am. Ceram. Soc.*, 1957, **40**, 74–80.
2. Komarneni, S. and Roy, D. M., Tobermorites: a family of cation exchangers. *Science*, 1983, **22**, 647–648.
3. Coleman, N. J., Synthesis, structure and ion exchange properties of 11 Å tobermorites from newsprint recycling residue. *Mater. Res. Bull.*, 2005, **40**, 2000–2013.
4. Coleman, N. J., Interactions of Cd(II) with waste-derived 11 Å tobermorites. *Sep. Purif. Technol.*, 2006, **48**, 62–70.
5. Reinik, J., Heinmaa, I., Mikkola, J.-P. and Kirso, U., Synthesis and characterisation of calcium-alumino-silicate hydrates from oil shale ash—towards industrial applications. *Fuel*, 2008, **87**, 1998–2003.
6. Mostafa, N. Y., Shaltout, A. A., Omar, H. and Abo-El-Enein, S. A., Hydrothermal synthesis and characterization of aluminium and sulfate substituted 1 1 nm tobermorites. *J. Alloys Compd.*, 2009, **467**, 332–337.
7. Hamid, S. A., The crystal structure of the 11-Å natural tobermorite $Ca_{2.25}Si_3O_{7.5}(OH)_{1.5}] \cdot 1\ H_2O$. *Z. Kristallogr.*, 1981, **154**, 189–198.
8. Merlino, S., Bonaccorsi, E. and Armbruster, T., The real structure of tobermorite 11 Å: normal and anomalous forms, OD character and polytypic modifications. *Eur. J. Mineral.*, 2001, **13**, 577–590.
9. Lin, K., Chang, J. and Cheng, R., *In vitro* hydroxyapatite forming ability and dissolution of tobermorite nanofibers. *Acta Biomater.*, 2007, **3**, 271–276.
10. Lansdown, A. B. G., Silver in health care: antimicrobial effects and safety in use. *Curr. Probl. Dermatol.*, 2006, **33**, 17–34.
11. Thom, D. C., Davies, J. E., Santerre, J. P. and Friedman, S., The haemolytic and cytotoxic properties of a zeolite-containing root filling material *in vitro*. *Oral Surg. Oral Med. Oral Pathol. Oral Radiol. Endod.*, 2003, **95**, 101–108.
12. Haile, T., Nakhla, G. and Allouche, E., Evaluation of the resistance of mortars coated with silver-bearing zeolite to bacterial-induced corrosion. *Corros. Sci.*, 2008, **50**, 713–720.
13. Ishitani, T., Active packaging for food quality preservation in Japan. In *Food and Food Packaging Materials—Chemical Interactions*, ed. P. Ackermann, M. Jagerstad and T. Ohlsonn. Royal Society of Chemistry, Cambridge, 1995, pp. 177–188.
14. Quintavalla, S. and Vicini, L., Antimicrobial food packaging in meat industry. *Meat Sci.*, 2002, **62**, 373–380.
15. Huang, H. and Yang, Y., Preparation of silver nanoparticles in inorganic clay suspensions. *Compos. Sci. Technol.*, 2008, **68**, 2948–2953.
16. Bright, K. R., Gerba, C. P. and Rusin, P. A., Rapid reduction of *Staphylococcus aureus* populations on stainless steel surfaces by zeolite ceramic coatings containing silver and zinc ions. *J. Hosp. Infect.*, 2002, **52**, 307–309.
17. Top, A. and Ülkü, S., Silver, zinc, and copper exchange in a Na-clinoptilolite and resulting effect on antibacterial activity. *Appl. Clay Sci.*, 2007, **24**, 13–19.
18. Bellantone, M., Coleman, N. J. and Hench, L. L., Bacteriostatic action of a novel four-component bioactive glass. *J. Biomed. Mater. Res.*, 2000, **51**, 484–490.
19. Bellantone, M., Coleman, N. J. and Hench, L. L., A novel sol–gel derived bioactive glass featuring antibacterial properties. *Key Eng. Mater.*, 2001, **192–195**, 597–600.
20. Ahmed, I., Ready, D., Wilson, M. and Knowles, J. C., Antimicrobial effect of silver-doped phosphate-based glasses. *J. Biomed. Mater. Res. A.*, 2006, **79**, 618–626.
21. Alt, V., Bechert, T., Steinrücke, P., Wagener, M., Seidel, P., Dingeldein, E., Domann, E. and Schnettler, R., An *in vitro* assessment of the antibacterial properties and cytotoxicity of nanoparticulate silver bone cement. *Biomaterials*, 2004, **25**, 4383–4391.
22. Maneerung, T., Tokura, S. and Rujiravanit, R., Impregnation of silver nanoparticles into bacterial cellulose for antimicrobial wound dressing. *Carbohydr. Polym.*, 2008, **72**, 43–51.
23. Bakumov, V., Gueinzius, K., Hermann, C., Schwarz, M. and Kroke, E., Polysilazane-derived antibacterial silver-ceramic nanocomposites. *J. Eur. Ceram. Soc.*, 2007, **27**, 3287–3292.
24. Ma, Z. J. and Yamaguchi, M., Stimulatory effect of zinc on deoxyribonucleic acid synthesis in bone growth of newborn rats: enhancement with zinc and insulin-like growth factor—I. *Calcif. Tissue Int.*, 2001, **69**, 158–163.
25. Tapiero, H. and Tew, K. D., Trace elements in human physiology and pathology: zinc and metallothioneins. *Biomed. Pharmacother.*, 2003, **57**, 399–411.
26. Bonferoni, M. C., Cerri, G., de' Gennaro, M., Juliano, C. and Caramella, C., Zn^{2+}-exchanged clinoptilolite-rich rock as active carrier for antibiotics in anti-acne topical therapy. *In vitro* characterization and preliminary formulation studies. *Appl. Clay Sci.*, 2007, **36**, 95–102.
27. Coleman, N. J. and Brassington, D. S., Synthesis of Al-substituted 11 Å tobermorite from newsprint recycling residue: a feasibility study. *Mater. Res. Bull.*, 2003, **38**, 485–497.

28. Wu, F.-G., Tseng, R.-L. and Juang, R.-S., Kinetic modeling of liquid-phase adsorption of reactive dyes and metal ions on chitosan. *Water Res.*, 2001, **35**, 613–618.
29. Reddad, Z., Gerente, C., Andres, Y. and Le Clirec, P., Adsorption of several metal ions onto a low-cost biosorbent: kinetic and equilibrium studies. *Environ. Sci. Tech.*, 2002, **36**, 2067–2073.
30. Coleman, N. J., Brassington, D. S., Raza, A. and Mendham, A. P., Sorption of Co^{2+} and Sr^{2+} by waste-derived 11 Å tobermorite. *Waste Manage.*, 2006, **26**, 260–267.
31. Ho, Y. S. and McKay, G., Pseudo-second order model for sorption processes. *Process Biochem.*, 1999, **34**, 451–465.
32. Azizian, S., Kinetic models of sorption: a theoretical analysis. *J. Coll. Interface Sci.*, 2004, **276**, 47–52.
33. Shaw, S., Henderson, C. M. B. and Komanschek, B. U., Dehydration/recrystallization mechanisms, energetics, and kinetics of hydrated calcium silicate minerals: an *in situ* TGA/DSC and synchrotron radiation SAXS/WAXS study. *Chem. Geol.*, 2000, **167**, 141–159.
34. Wieker, W., Grimmer, A.-R., Winkler, A., Mägi, M., Tarmak, M. and Lippmaa, E., Solid-state high-resolution ^{29}Si NMR spectroscopy of synthetic 14 Å, 11 Å and 9 Å tobermorites. *Cem. Concr. Res.*, 1982, **12**, 333–339.
35. Cong, X. and Kirkpatrick, R., ^{29}Si and ^{17}O NMR investigation of the structure of some crystalline calcium silicate hydrates. *Adv. Cem. Based Mater.*, 1996, **3**, 133–143.
36. Zhao, D., Zhou, J. and Liu, N., Preparation and characterization of Mingguang palygorskite supported with silver and copper for antibacterial behavior. *Appl. Clay Sci.*, 2006, **33**, 161–170.
37. Magaña, S. M., Quintana, P., Aguilar, D. H., Toledo, J. A., Ángeles-Chávez, C., Cortés, M. A., León, L., Freile-Pelegrín, Y., López, T. and Torres Sánchez, R. M., Antibacterial activity of montmorillonites modified with silver. *J. Mol. Catal. A: Chem.*, 2008, **281**, 192–199.
38. De la Rosa-Gomez, I., Olguín, M. T. and Alcántara, D., Bactericides of coliform microorganisms from wastewater using silver-clinoptilolite rich tuffs. *Appl. Clay Sci.*, 2008, **40**, 45–53.
39. Mozgawa, W. and Bajda, T., Application of vibrational spectra in the studies of cation sorption on zeolites. *J. Mol. Struct.*, 2006, **792–793**, 170–175.
40. Pehlivan, H., Balköse, D., Ülkü, S. and Tihminlioglu, F., Characterization of pure and silver exchanged natural zeolite filled polypropylene composite films. *Compos. Sci. Technol.*, 2005, **65**, 2049–2058.
41. Donia, A. M., Atia, A. A. and Elwakeel, K. Z., Recovery of gold(III) and silver(I) on a chemically modified chitosan with magnetic properties. *Hydrometallurgy*, 2007, **87**, 197–206.
42. Lu, S., Gao, W. and Gu, H. Y., Construction, application and biosafety of silver nanocrystalline chitosan wound dressing. *Burns*, 2008, **34**, 623–628.
43. Ma, Y., Zhou, T. and Zhao, C., Preparation of chitosan–nylon-6 blended membranes containing silver ions as antibacterial materials. *Carbohydr. Res.*, 2008, **343**, 230–237.
44. Benhammou, A., Yaacoubi, A., Nibou, L. and Tanouti, B., Adsorption of metal ions onto Moroccan stevensite: kinetic and isotherm studies. *J. Coll. Interface Sci.*, 2005, **282**, 320–326.
45. Purna Chandra Rao, G., Satyaveni, S., Ramesh, A., Seshaiah, K., Murthy, K. S. N. and Choudary, N. V., Sorption of cadmium and zinc from aqueous solutions by zeolite 4A, zeolite 13X and bentonite. *J. Environ. Manage.*, 2006, **81**, 265–272.
46. El-Kamash, A. M., Zaki, A. A. and Abed El Geleel, M., Modeling batch kinetics and thermodynamics of zinc and cadmium ions removal from waste solutions using synthetic zeolite A. *J. Hazard. Mater.*, 2005, **B127**, 211–220.
47. Kokubo, T. and Takadama, H., How useful is SBF in predicting in vivo bone bioactivity? *Biomaterials*, 2006, **27**, 2907–2915.
48. Ramasubbu, A., Vanangamudi, A., Muthusubramanian, S., Ramachandran, M. S. and Sivasubramanian, S., Electrocatalytic studies using silver-clay composite—a novel material. *Electrochem. Commun.*, 2000, **2**, 56–64.
49. Difang Zhao, D., Zhou, J. and Liu, N., Surface characteristics and photoactivity of silver-modified palygorskite clays coated with nanosized titanium dioxide particles. *Mater. Charact.*, 2007, **58**, 249–255.